The North Polar Spur and Aquila Rift

Yoshiaki Sofue★

Institute of Astronomy, University of Tokyo, Mitaka, Tokyo 181-0015, Japan

ABSTRACT

Soft X-ray intensity at 0.89 keV along the North Polar Spur (NPS) is shown to follow the extinction law due to the interstellar gas in the Aquila Rift by analysing the *ROSAT* archival data, which proves that the NPS is located behind the rift. The Aquila–Serpens molecular clouds, where the X-ray optical depth exceeds unity, are shown to have a mean LSR velocity of $v = 7.33 \pm 1.94\,\mathrm{km\,s^{-1}}$, corresponding to a kinematic distance of $r = 0.642 \pm 0.174\,\mathrm{kpc}$. Assuming a shell structure, a lower limit of the distance to NPS is derived to be $1.01 \pm 0.25\,\mathrm{kpc}$, with the shell centre being located farther than 1.1 kpc. Based on the distance estimation, we argue that the NPS is a Galactic halo object.

Key words: ISM: individual objects: North Polar Spur – ISM: individual objects: Aquila Rift – ISM: kinematics and dynamics – Galaxy: centre – radio lines: ISM – X-rays: diffuse background.

1 INTRODUCTION

The North Polar Spur (NPS) is defined as the prominent ridge of radio continuum emission, emerging from the galactic plane at $l \sim 20°$ towards the North Galactic Pole (Haslam et al. 1982; Page et al. 2007). The spur is also prominent in soft X-rays as shown in the Wiskonsin and *ROSAT* all-sky maps (McCammon et al. 1983; Snowden et al. 1997).

Discovery of the *Fermi* γ-ray bubbles (Su, Slatyer & Finkbeiner 2010) has drawn attention to energetic activities in the Galactic Centre, and possible relation of the NPS to the *Fermi* bubbles has been pointed out (Kataoka et al. 2013; Mou et al. 2014). The underlying idea is that the NPS is a shock front produced by an energetic event in the Galactic Centre with released energy of the order of $\sim 10^{55-56}$ erg (Sofue 1977, 1984, 1994, 2000; Bland-Hawthorn & Cohen 2003). In this model, the distance to NPS is assumed to be ~ 7 kpc.

On the other hand, there have been traditional models to explain the NPS by local objects such as a nearby supernova remnant, hypernova remnant, or a wind front from massive stars (Berkhuijsen, Haslam & Salter 1971; Egger & Aschenbach 1995; Willingale et al. 2003; Wolleben 2007; Puspitarini et al. 2014). In these models, the distance to NPS is assumed to be several hundred pc.

Hence, the distance is a crucial key to understand the origin of NPS. In this paper, we revisit this classical problem, and give a constraint on the distance of NPS, following the method proposed by Sofue (1994).

We adopt the common idea as the working hypothesis that the NPS is a part of a shock front shell composed of high-temperature plasma and compressed magnetic fields, emitting both the X-ray

and synchrotron radio emissions. For the analysis, we use the archival data of *ROSAT* All Sky X-ray Survey (Snowden et al. 1997), Argentine–Bonn–Leiden All Sky H I Survey (Kalberla et al. 2005), and Colombia Galactic Plane CO Survey (Dame, Hartman & Thaddeus 2001).

2 THE NPS IN SOFT X-RAYS

Fig. 1 shows a colour-coded map of X-ray intensities in a $\pm 50°$ region around the Galactic Centre obtained by using the *ROSAT* archival data, where red represents the *R*2 (0.21 keV)-band intensity, green for *R*5 (0.89 keV), and blue for *R*7 (1.55 keV). The dashed lines trace the loci along which the analysis of X-ray absorption was obtained in this paper. The central locus below $b \sim 15°$ was drawn along the radio continuum spur traced in the 1.4 GHz map by Sofue & Reich (1979). The white dashed line is a contour along which the optical depth of *R*5-band emission due to the interstellar gas is equal to unity.

Here, we chose *R*2, *R*5 and *R*7 bands in order to cover as wide range of X-ray energies as possible to see the variation of optical depths corresponding to strongly varying interstellar gas densities. We used *R*5 band as the representative of *R*4, *R*5 and *R*6 bands, because the three bands are largely overlapping. The X-ray emission from the NPS is shown to be originating from hot plasma of temperature $\sim 10^{6.3}$–$10^{6.5}$ K (Snowden et al. 1997). Table 1 shows the energy bands of *ROSAT* observations.

3 THE AQUILA RIFT COMPOSED OF H I AND H_2 GASES

The Aquila Rift was originally known as a giant dark lane dividing the starlight Milky Way by heavy extinction (Weaver 1949; Arendt

★ E-mail: sofue@ioa.s.u-tokyo.ac.jp
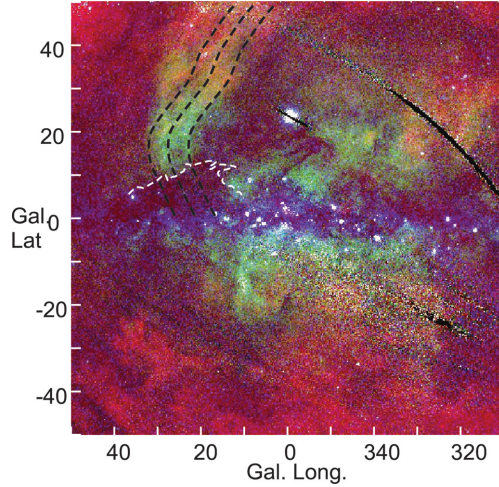
Figure 1. Colour-coded X-ray map with red for *R2* (0.21 keV), green for *R5* (0.89 keV), and blue for *R7* (1.55 keV), as obtained using the *ROSAT* archival data (Snowden et al. 1997). The three dashed lines trace the NPS at the outer edge, peak intensity ridge, and inner region, along which the absorption analysis is obtained. The white dashed line indicates a contour along which the optical depth of *R5* (0.89 keV)-band emission due to the interstellar gas is equal to unity ($\tau_5 = 1$, or $N = N_5$).

et al. 1998; Dobashi et al. 2005). We analyse the distribution of interstellar H I and H$_2$ gases in the Aquila Rift, and investigate the relation to absorption features of the X-ray NPS. We use the Leiden–Argentine–Bonn All Sky H I Survey (Kalberla et al. 2005) and Colombia Galactic Plane CO Survey (Dame et al. 2001).

Fig. 2 shows the distribution of column density of total hydrogen atoms $N = N(\text{H}) + 2N(\text{H}_2)$ obtained from integrated intensities of the H I and CO lines. The integrations were obtained in the whole velocity ranges: H I line from -200 to $+200$ km s^{-1}, and CO line

Table 1. *ROSAT* X-ray bands and critical column density of H atoms (Snowden et al. 1997).

i	Band	E range (keV)	Mean E (keV)	N_i ($\tau_i = 1$) (10^{20} H cm^{-2})
1	*R1*	0.11–0.28	0.195	0.73
2	*R2*	0.14–0.28	0.21	1.41
4	*R4*	0.44–1.01	0.725	23.0
5	*R5*	0.56–1.21	0.885	27.0
6	*R6*	0.73–1.56	1.145	36.0
7	*R7*	1.05–2.04	1.545	90.0
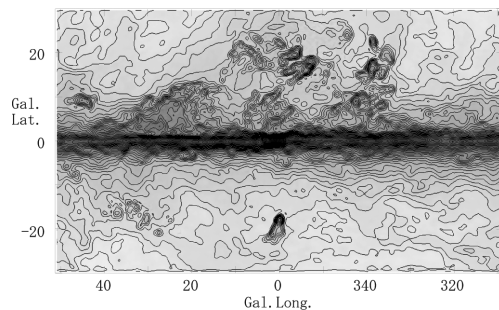
Figure 2. Hydrogen column density, $N = N(\text{H I}) + 2N(\text{H}_2)$, produced from the H I and CO line survey data by Kalberla et al. (2005) and Dame et al. (2001). Contour levels are logarithmic from 0 to 6686×10^{23} H cm^{-2} by exp(1/50) steps.

from -300 to $+300$ km s^{-1}. Hence, the map shows the column density along the entire line of sight. Prominent in these maps is the tilted ridge of H I and H$_2$ gases associated with the Aquila Rift.

The hydrogen column density along the line of sight was calculated by

$$N = C_{\text{H I}} I_{\text{H I}} + 2 C_{\text{H2}} I_{\text{CO}}, \tag{1}$$

where $I_{\text{H I}}$ and I_{CO} are the integrated intensities of H I and ^{12}CO(1–0) lines, and we adopt the conversion factors of $C_{\text{H I}} = 1.82 \times 10^{18}$[H cm^{-2}/K km^{-1}] and $C_{\text{H2}} = 2.0 \times 10^{20}$[H$_2$ cm^{-2}/K km^{-1}].

4 ABSORPTION OF X-RAYS BY AQUILA RIFT

4.1 Latitude variation of X-ray optical depth

Table 1 and Fig. 3 show energy dependence of the critical column density, N_i, at which the optical depth defined by

$$\tau_i = N / N_i, \tag{2}$$

is equal to unity ($i = 1, 2, \ldots, 7$ corresponding to $R1, R2, \ldots, R7$, respectively), as obtained from Snowden et al. (1997). Typical critical densities used in this paper are $N_2 = 1.4 \times 10^{20}$ H cm^{-2}, $N_5 = 27.0 \times 10^{20}$ H cm^{-2}, and $N_7 = 90.0 \times 10^{20}$ H cm^{-2}.

If X-rays in the ith band are emitted at a distance x with an intrinsic intensity I_i^0, they are absorbed by the intervening interstellar gas, and yield the observed intensity

$$I_i = I_i^0 \exp(-\tau_i) + I_i^f, \tag{3}$$

where I_i^f is the foreground emission.

In Fig. 4, we plot *R5*-band intensities (*ROSAT* count rate s^{-1} arcmin^{-1}) against latitude in comparison with the total column density of hydrogen atoms along the three dashed loci indicated in Fig. 1. The middle panel shows the plot along the NPS peak ridge (central locus), while the top panel for the eastern locus at $\delta l = +5°$ along the outer edge of NPS, and the bottom for the western (inner) locus at $\delta l = -5°$.

Each plotted value is the mean of *R5*-band count rates in a box of extent $(\Delta l \times \Delta b) = (2° \times 1°)$ at every 1° latitude interval along the loci. Long thin bars represent standard deviation s_d about the mean
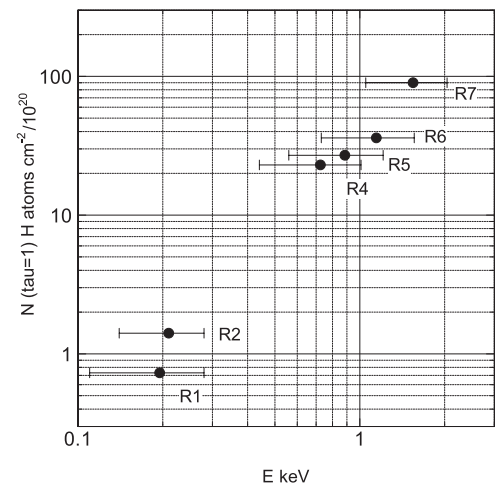

Figure 3. Critical hydrogen column density N_i as a function of X-ray energy plotted for the *ROSAT* energy bands obtained by using the data by Snowden et al. (1997).
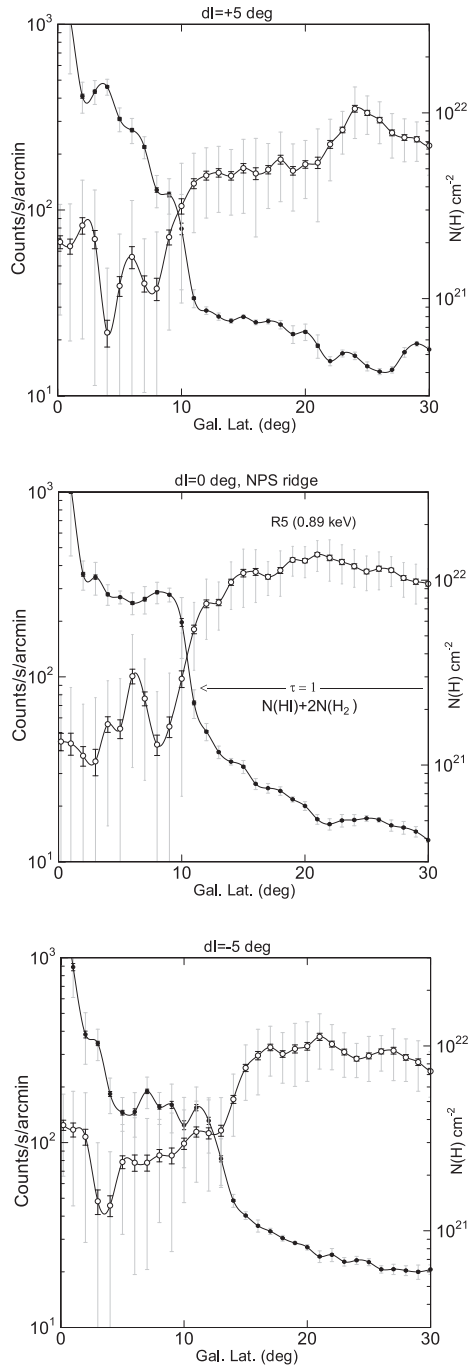
Figure 4. *R*5-band (0.89 keV) intensity (in *ROSAT* count rate s^{-1} arcmin^{-1}) compared with total H column density, $N = N(\text{H\,I}) + 2N(\text{H}_2)$, along the dashed lines in Fig. 1) plotted against b. From top to bottom: outer edge shifted by $\delta l = +5°$ to the east, along the peak ridge at $\delta l = 0°$, and inside NPS at $\delta l = -5°$. Long and short bars represent s_d and s_e, respectively.

value in each box. Short thick bars are standard errors, $s_e = s_d/\sqrt{n}$, with $n \sim 55$ being the number of data points in each box.

The figure shows that the *R*5-band X-ray intensity is inversely correlated with the H column density. The intensity along the NPS peak ridge (middle panel) starts to decrease at $b = 15°$ showing a shoulder-like drop, and falls by $1/e$ at $b = 11°$, at which the H atom column density is $N = 2.7 \times 10^{21}$ H cm^{-2}, coinciding with threshold value N_5 corresponding to $\tau_5 = 1$. Similarly, a shoulder-
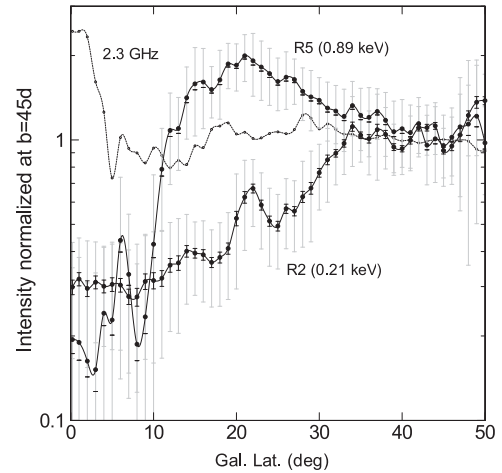
Figure 5. Variations of relative X-ray intensities in *R*2 and *R*5 bands, and 2.3 GHz radio continuum brightness plotted along the NPS ridge against galactic latitude. Intensities are normalized at $b \simeq 45°$. Long and short bars represent s_d and s_e, respectively.

like drop appears at $b \simeq 10°$ along the outer edge (top panel), and at $b \simeq 16°$ along the inner locus (bottom panel). Thus, the lower is the longitude, the higher is the latitude of the shoulder position.

The steepest decreasing point of X-rays in each panel coincides with the position at which the H column density is equal to the critical value $N = N_5 = 2.7 \times 10^{21}$ H cm^{-2}, where $\tau_5 = 1$. Namely, *R*5-band X-rays of NPS fade away near the white dashed contour in Fig. 1 in coincidence with the distribution of dark clouds in the Aquila Rift.

In Fig. 5, we show the variation of *R*5- and *R*2-band intensity as a function of galactic latitude along the spur ridge. The X-ray intensity is normalized to the value at $b = 45°$ in each band. We also plot radio continuum intensity at 2.3 GHz using the Rhodes radio survey data by Jonas, Baart & Nicolson (1998) after background filtering (Sofue & Reich 1979). The *R*2 intensity is strongly absorbed already at latitudes as high as $45°$, where the H atom column density is $N \sim 4 \times 10^{20}$ H cm^{-2} exceeding the threshold value of $N_2 = 1.4 \times 10^{20}$ H cm^{-2}, indicating $\tau_2 > 3$.

### 4.2 Extinction law along the NPS

Fig. 6 shows *R*5-band intensity and H column density plotted against latitude in linear scale. We also show an extinction curve corresponding to the hydrogen column density, where the plotted values are proportional to $\exp(-\tau_5)$ and normalized to the *R*5-band intensity at $b \sim 20°$. Here, $\tau = N/N_5$ and $N_5 = 27.0 \times 10^{20}$ H cm^{-2}. The X-ray intensity follows almost exactly the extinction curve.

In Fig. 7, we plot *R*5-band intensity along NPS at $b < 30°$ as a function of the optical depth τ_5. Here, the minimum value of intensity at $b \sim 5°$ was subtracted as the foreground emission I_5^f, and the intensity is normalized by the maximum value at $b \sim 20°$. The inserted line shows the extinction law following an equation

$$I_5 = I_0 \exp(-\tau_5), \tag{4}$$

where I_0 is the maximum intensity.

The observed relations shown in Figs 4–7 indicate that the X-ray intensity follows the simplest extinction law, and show that the NPS is indeed absorbed by the interstellar gas in the Aquila Rift region. The facts also prove that the NPS is an intrinsically continuous
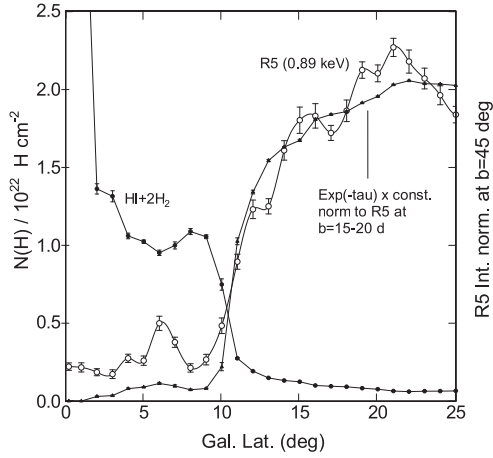
Figure 6. Relative *R5*-band intensity (circle) compared with the total hydrogen column density (dot) at $b < 25°$. Triangles show the extinction profile proportional to $\exp(-\tau_5)$ normalized to the *R5*-band intensity at $b \sim 20°–25°$. Bars are standard errors.
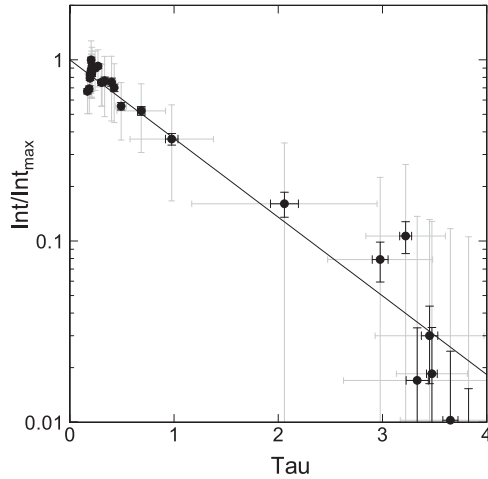
Figure 7. *R5*-band intensities at $b < 30°$ plotted as a function of optical depth. The intensity is normalized by the maximum value at $b \sim 20°$ with the minimum value at $b \sim 5°$ being subtracted. The optical depth was calculated by $\tau = N/N_5$ with $N_5 = 27.0 \times 10^{20}$ H cm^{-2}. The straight line represents the extinction law, $I/I_0 = \exp(-\tau_5)$. Long and short bars denote s_d and s_e, respectively.

structure emitting X-rays even below latitudes at which the optical depth is greater than unity.

This is consistent with our working hypothesis that the NPS is a continuous structure tracing the radio NPS. On the other hand, it denies the possibility that NPS has a real emission edge near $b \sim 11°$, in which case the correlations in Figs 6 and 7 are hard to be explained.

5 DISTANCE OF ABSORBING NEUTRAL GAS

5.1 Kinematical distance from LSR velocity

A lower limit distance of NPS can be obtained by analysing the kinematical distance of the absorbing H I and molecular gases. The distance of the gas r is related to the radial velocity v_r as

$$r = v_r/(A \sin 2l \cos b), \quad (5)$$
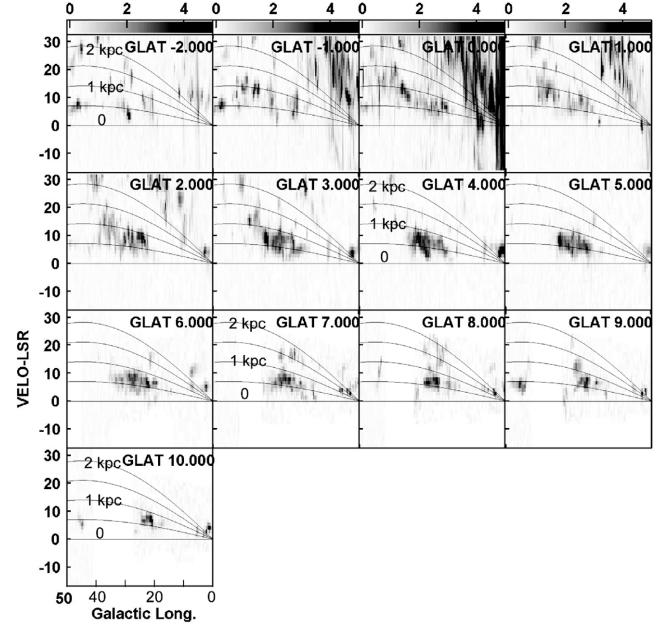
Figure 8. CO-line LV diagrams for $l = 0°–50°$ at different latitudes from data by Dame et al. (2001). Inserted thin lines indicate kinematic LSR velocities corresponding to distances 0, 0.5, 1, 1.5, and 2 kpc from the Sun. This figure, therefore, represents approximate cross-sections of the Aquila Rift at different latitudes as seen from the Galactic North Pole.

where *A* is Oort's constant. We here adopt the IAU recommended value $A = 14.4$ km s^{-1} kpc^{-1}.

Fig. 8 shows CO line longitude-velocity (LV) diagrams at several galactic latitudes in the Aquila Rift region. The diagrams show a prominent clump at around $v_r \sim 7$ km s^{-1} and $l \sim 25°$. A corresponding feature is recognized in the H I LV diagram as a valley of emission at the same LV position at $b \simeq 5°$, indicating that the CO Aquila Rift is surrounded by an H I gas envelope. However, the H I diagrams were too complicated for distance estimation of the Aquila Rift, and were not used here.

In the CO LV diagram (Fig. 8), we insert thin lines showing velocities corresponding to distances of 0, 0.5, 1, 1.5, and 2 kpc, as calculated by equation (5). The major CO Aquila Rift is thus shown to be located at a distance of $r = 0.6–0.7$ kpc with the nearest and farthest edges being at 0.3 and 1 kpc, respectively. At $b \sim 8°$ an extended spur, reaching $v_r \sim 20$ km s^{-1}, seems to be associated with the major ridge, whose kinematical distance is estimated to be as large as $r \sim 1.8$ kpc. This figure, therefore, represents cross-sections of the Aquila Rift at different latitudes as seen from the Galactic North Pole.

Fig. 9 shows CO line spectra towards the densest region in the Aquila Rift. Each line profile includes velocity information mixed with the cloud motion and velocity dispersion. The velocity dispersion is of the order of a few km s^{-1}, but is difficult to separate from the kinematical component.

We, therefore, used peak velocities of individual spectra. We read the peak velocities in the spectra shown in Fig. 9 from $l = 22°$ to $32°$ and from $b = 3°.62$ to $7°.36$. If a spectrum had two peaks, we adopted two corresponding velocities. Thus, we obtained 44 peak velocities. We then calculated kinematical distance for each measured velocity using equation (5). The measured velocities and calculated distances were averaged to obtain a mean velocity and distance as follows:

$$v = 7.33 \pm 1.94(0.29) \text{ km s}^{-1} \quad (6)$$
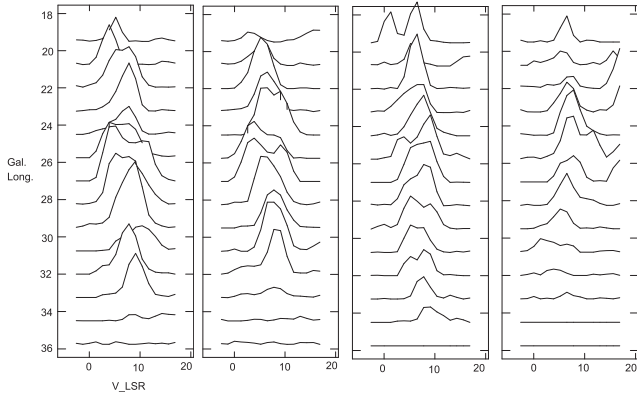
Figure 9. CO line spectra at latitudes $b = 3°62, 4°87, 6°12,$ and $7°37$ (from left to right) with longitude interval of about $2°$. The ordinate tick interval corresponds to the CO-line brightness temperature of 2 K.

and

$$r = 0.642 \pm 0.174(0.026)\,\mathrm{kpc}, \tag{7}$$

where the former errors are the standard deviation s_d, and the latter in the parenthesis are the standard errors of the mean values $s_e = s_d/\sqrt{n}$ with $n = 44$. Since the measured velocities represent real motions of individual clouds, we adopt here the standard deviations as the errors of the mean velocity and distance.

We comment on possible systematic errors in the used parameters for calculation of kinematic distance. The Oort constant A still includes uncertainty of $\sim$10 per cent. The solar motion may include $\sim$1 km s^{-1} uncertainty to cause systematic errors of several per cent in LSR velocities. Also, interstellar turbulent motion may apply to the molecular clouds, yielding a few km s^{-1} uncertainties in kinematical velocities. These uncertainties may cause a systematic error of $\sim$20–30 per cent in the derived distance.

5.2 Comparison with optical extinction

Weaver (1949) showed that the colour excess of stars towards Aquila Rift starts to increase at a distance modulus $m - M \sim 6$–8 mag, reaching a local maximum at $m - M \sim 8.5$–9. This indicates that the front edge of the dark cloud is at a distance of $r \sim 200$ pc, and attains maximum density at $\sim$500 pc. Straižys Černis & Bartašiūtė (2003)

showed that the front edge of Aquila Rift is located at $r = 225 \pm 55$ pc, where the visual extinction A_V starts to increase, and reaches a maximum at $r \sim 600$ pc.

A more number of measurements are summarized in Dzib et al. (2010). Most of the measurements are towards the Serpens molecular cloud and/or core at $(l, b) = (31°4, 5°5)$. We reproduce their compilation in Table 2, where we added our new estimations using the data from the literature. The listed distances to Aquila Rift (Serpens cloud) are distributed from 200 to 650 pc. By averaging the listed values, we obtain a distance of $r = 430 \pm 147$ pc.

Optical measurements yielded systematically smaller distances compared to the radio line kinematics and VLBI parallax measurements (Dzib et al. 2010). The latter is consistent with the present CO line kinematical distance. The difference between optical and radio measurements would be due to selection effect of optical observations, in which stars are heavily absorbed so that farther stars are harder to be observed.

5.3 The molecular core of Aquila Rift

From the spectrum, we estimate the integrated CO intensity to be about $I_{CO} \sim 20$ K km s^{-1}, which yields a column density of hydrogen molecules of 4×10^{21} H$_2$ cm^{-2}, or hydrogen atom column density of 8×10^{21} H cm^{-2}. This is about equal to the critical column density for $R7$ band, $N_7 = 9 \times 10^{21}$ H cm^{-2}, indicating that the $R7$-band emission is marginally absorbed by the Serpens clouds.

CO gas in the Aquila Rift is distributed from $b = 0°$ to $10°$ and from $l = 20°$ to $30°$. For a mean distance to the ridge centre of 0.642 kpc, the area is approximated by a rectangular triangle with one side length of $s \sim 100$ pc. Taking an average column density through the ridge of $N \sim 8 \times 10^{21}$ H cm^{-2}, we estimate the cloud's mass to be $M \sim (s^2/2)m_H N \sim 3 \times 10^5$ M$_\odot$. Hence, the Aquila Rift is considered to be a giant molecular cloud of medium size and mass, enshrouded in an extended H I gas.
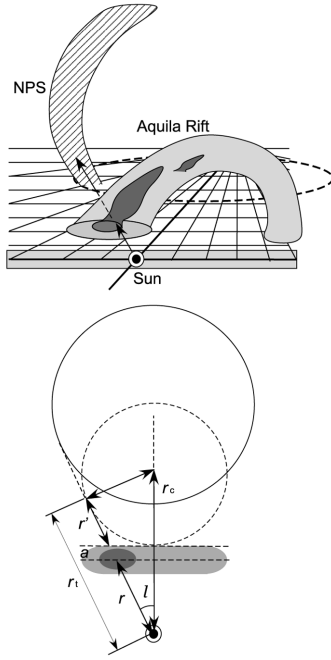
If we assume a line-of-sight depth of the cloud to be $\sim$100 pc, the volume density of gas is of the order of $\sim$26 H cm^{-3}, lower than that of a typical giant molecular cloud. Taking a half velocity width $\sigma_v \sim 4$ km s^{-1} and radius $a \sim 50$ pc, the Virial mass is estimated to be of the order of $M_V \sim \sigma_v^2 a/G \sim 2 \times 10^5$ M$_\odot$. Hence, the Aquila molecular cloud will be a gravitationally bound system, although the gravitational equilibrium assumption may not be a good approximation because of its complicated shape.

Table 2. Distances to the Aquila–Serpens Rift.[a]

Authors	r (pc)	Method
Weaver (1949)[b]	450 ± 100	A_v opt
Racine (1968)	440	A_v opt
Strom, Grasdalen & Strom (1974)	440	A_v IR
Chavarria et al. (1988)	245 ± 30	A_v opt/IR
Zhang et al. (1988)	650 ± 180	A_v opt/IR
ibid	600	Kin. CO, NH$_3$
de Lara, Chavarria & Lopez-Molina (1991)	311 ± 38	A_v opt
Straižys, Černis & Bartašiūtė 2003	259 ± 37	A_v; front edge
ibid[b]	500 ± 50	A_v
Dzib et al. (2010)	415 ± 25	Maser parallax
Knude (2011)	203 ± 7	A_v 2MASS, 1st peak
ibid[b]	400 ± 50	ibid, 2nd peak
This work[b]	642 ± 174	Kin. $l = 20°$–$30°$, $b = 3°$–$8°$
Average[b]	430 ± 147	

Notes. [a]After Dzib et al. (2010) for Serpens cloud.
[b]Our estimations.

Table 3. Lower limit distance of the NPS.

Method	Distance (kpc)
CO-line kin. dist. (This work)	1.01 ± 0.25 kpc
Using the average in Table 2	0.70 ± 0.24 kpc
Radio depolarization (Sun et al. 2014)	~ 2–3 kpc
Faraday rotation (This work)	~ 5 kpc

6.1 Comparison with Faraday distances of NPS

Sun et al. (2014) analysed Faraday screening of linearly polarized radio continuum emission towards the low-latitude extension of NPS ridge. They concluded that the beam depolarization at 2.3 GHz indicates that the NPS ridge is located farther than 2–3 kpc.

They also showed that the B vectors at 4.8 GHz are aligned at position angles $\phi_1 \simeq 40°$ towards the most strongly polarized region at $(l, b) = (22°7, 4°0)$, whereas 2.3-GHz B vectors are aligned at $\phi_2 = -40°$. The values of rotation measure, *RM*, of extragalactic radio sources are $RM \sim +50$ to $+100$ rad m^{-2} in the same direction of $l = 23°$ to $25°$, $b = 3°$ to $5°$ (Taylor, Stil & Sunstrum 2009). Hence, we may choose a positive minimum rotation of the polarization angle to yield $\Delta\phi = +100°$. This results in a rotation measure of $RM = \Delta\phi/(\lambda_2^2 - \lambda_1^2) \sim +130$ rad m^{-2}.

If we take interstellar electron density of $n_e \sim 10^{-2}$ cm^{-2} and magnetic field of $B \sim 3$ μG, the estimated RM corresponds to a line-of-sight depth of $r = |RM|/(0.82 n_e B) \sim 5$ kpc. The corresponding height is 300 to 400 pc from the galactic plane, beyond which the Faraday rotation would be negligible. Hence, the here estimated value is a lower distance. In Table 3, we summarize the estimated lower limits to the distance of NPS.

6.2 Effect of the bulge

Galactic bulge emission may be superposed on the used *ROSAT* maps, producing an absorption band along the galactic plane, particularly in the Galactic Centre direction. Although the bulge emission in the analysed region at $l \sim 20°$–30°, $b \sim 10°$–50° has not been thoroughly investigated, it will be weaker than the NPS emission. Hence, the present result gives a lower limit to the X-ray emitting source of the NPS possibly superposed by weak bulge emission. However, this does not affect the present result, because the lower limit applies both to the distances of NPS and superposed emissions.

7 CONCLUSION AND DISCUSSION

7.1 Summary

We summarize the major results as follows.

(1) Soft X-rays from the NPS are absorbed by the galactic disc, specifically by dense clouds in the Aquila Rift, as evidenced by (A) the clear anticorrelation between *R5* (0.89 keV) X-ray intensity and total H column density; and (B) the coincidence of *R5*-band intensity profile with the interstellar extinction profile, indicating that the soft X-rays obey the extinction law due to Aquila Rift gas.

(2) The kinematical distance to the absorbing gas in the Aquila Rift was measured to be $r = 642 \pm 174$ pc. Assuming a shell structure, the lower limit to the NPS ridge is estimated to be 1.02 ± 0.25 kpc.

(3) The derived distance shows that the major part of the NPS is located high above the galactic gas layer, and we conclude that the

Figure 10. Schematic relationship between NPS and Aquila Rift. The dashed circle shows the nearest possible case for calculating a lower limit distance.

In order to lift the cloud to the height of $h \sim r \tan 5° \sim 50$ pc from the galactic plane, gravitational energy of $E_g \sim 10^{50}$ erg is required. The origin of Aquila Rift in relation to its inflating-arch morphology lifted from the galactic plane would be an interesting subject for the future, particularly in relation to magnetic fields.

6 THE DISTANCE OF NPS

We now estimate a lower limit of the distance to NPS, assuming that the NPS is a part of a shell. The nearest allowed configuration of the shell with respect to the Aquila Rift is illustrated in the lower panel of Fig. 10. In the nearest possible case shown by the dashed circle, the shell is in touch with the farthest edge of the Aquila Rift. Here, the shell centre is assumed to be located in the direction of $l \sim 0°$. Let the distance of the tangential point of the shell r_t, the distance to the shell centre r_c, and the half thickness of the Aquila Rift on the line of sight a. Then, the distance r_t and r_c are related to the distance of the Aquila Rift ridge r as

$$r_t \simeq r + a + r' = (r + a)(1 + \sin l) \qquad (8)$$

and

$$r_c \simeq r_t / \cos l. \qquad (9)$$

We take the determined distance of the molecular Aquila Rift, $r = 0.642 \pm 0.174$ kpc, and assume a line-of-sight width of 100 pc, or a radius $a \simeq 50$ pc, for the rift ridge at $l \sim 27°$. Then, we have a lower limit distance to the NPS as $r_t \sim 1.01 \pm 0.25$ kpc, and to the shell centre $r_c \sim 1.13 \pm 0.29$ kpc. If we use the averaged value of measured distances to Aquila Rift as listed in Table 2, the lower limit distance to NPS would be farther than 0.70 ± 0.24 kpc, and the shell centre farther than 0.79 ± 0.27 kpc. If the shell centre is in the direction of $(l, b) \sim (330°, 20°)$, as Loop I fitting suggests, the distance should be greater.
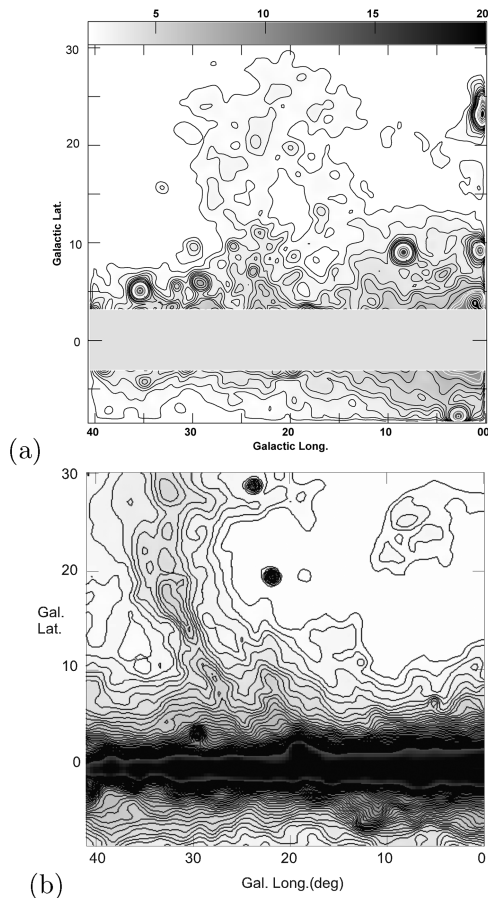
NPS is a galactic halo object. Since the gas density in the halo is too small to cause further absorption, the NPS distance is allowed to be much farther including the Galactic Centre distance.

7.2 Possible extinction-free NPS at low latitudes

We may speculate about a possible intrinsic structure of NPS by correcting for the absorption by accepting the present distance estimation. We here use the *ROSAT R*7 data where the extinction is smallest among the available bands, so that overcorrection is less significant than in other bands.

We, first smooth the *R*7 map by a Gaussian beam with $1°$ FWHM in order to increase the signal-to-noise ratio, and we divide it by a map of $\exp(-\tau_i) = \exp(-N/N_7)$ with $N_7 = 90.0 \times 10^{20}\,\mathrm{H\,cm^{-2}}$. Fig. 11 shows the thus obtained extinction-free *R*7-band map compared with the colour-coded X-ray map from Fig. 1. An X-ray spur is revealed to show up along at $b < 10°$. Note that the region nearer to the galactic plane at $|b| < 3°$ should not be taken seriously, where overcorrection due to the too large optical depth may exit. In the figure, we also compare the *R*7 map with a background-filtered 2300-MHz radio continuum map (Jonas et al. 1998).

Both the radio and X-ray spurs emerge from the galactic plane at about the same angle $\sim 50°$, and become sharper, narrower, and brighter towards the plane. The X-ray spur is displaced to inside

(westwards) of the radio ridge by $\sim 5°$, or $\sim 10–15$ per cent of the apparent curvature radius. The displacement is systematically observed over the entire NPS, and will be attributed to the difference of emitting mechanisms. We may also mention that the *Fermi* γ-ray bubble is located further inside the X-ray shell.

7.3 Origin of NPS

If the NPS is a shock front of an old supernova remnant, the radio brightness-to-diameter relation applied to Loop I indicates a diameter of ~ 100 pc and a distance to NPS of the same order (Berkhuijsen, Haslam & Salter 1971) An alternative model attributes the origin to a hypernova or multiple supernovae, or stellar wind from high-mass stars (Egger & Aschenbach 1995; Willingale et al. 2003; Wolleben 2007; Puspitarini et al. 2014). In this model, the distance to the NPS is assumed to be ~ 1 kpc, which is consistent with the present lower-limit distance. However, the model needs to explain the origin of an extraordinarily active star formation at altitudes as high as ~ 300 pc above the galactic disc.

The Galactic Centre explosion model postulates bipolar hyper-shells produced by a starburst 15 million years ago with explosive energy of the order of $10^{55–56}$ erg in the Galactic Centre (Sofue 1977, 1984, 1994, 2000; Bland-Hawthorn & Cohen 2003). A shock front is supposed to reach a radius ~ 10 kpc in the polar regions and ~ 3 kpc in the galactic plane. The lower limit distance, and the fact that the low-latitude narrow ridges in radio and X-rays emerge from the galactic plane are consistent with the Galactic Centre explosion model.

Figure 11. (a) Extinction-corrected *R*7 band X-ray map for the NPS region. Contours are from 70.4 by 17.6 count intervals in *ROSAT* count rate s^{-1} arcmin^{-1}. Region at $|b| < 3°$ is over-corrected, and should not be taken real. (b) Background-filtered 2.3 GHz map from Rodhes survey (Jonas et al. 1998) with contours every 0.05 Jy beam^{-1}.

REFERENCES

Arendt R. G. et al., 1998, ApJ, 508, 74
Berkhuijsen E., Haslam C., Salter C., 1971, A&A, 14, 252
Bland-Hawthorn J., Cohen M., 2003, ApJ, 582, 246
Chavarria K. C., de Lara E., Finkenzeller U., Mendoza E. E., Ocegueda J., 1988, A&A, 197, 151
Dame T. M., Hartman D., Thaddeus P., 2001, ApJ, 547, 792
de Lara E., Chavarria K. C., Lopez-Molina G., 1991, A&A, 243, 139
Dobashi K., Uehara H., Kandori R., Sakurai T., Kaiden M., Umemoto T., Sato F., 2005, PASJ, 57, 1
Dzib S., Loinard L., Mioduszewski A. J., Boden A. F., Rodríguez L. F., Torres R. M., 2010, ApJ, 718, 610
Egger R. J., Aschenbach B., 1995, A&A, 294, L25
Haslam C. G. T., Salter C. J., Stoffel H., Wilson W. E., 1982, A&AS, 47, 1
Jonas J. L., Baart E. E., Nicolson G. D., 1998, MNRAS, 297, 977
Kalberla P. M. W., Burton W. B., Hartmann D., Arnal E. M., Bajaja E., Morras R., Pöppel W. G. L., 2005, A&A, 440, 775
Kataoka et al., 2013, ApJ, 779, 57
Knude J., 2011, preprint (arXiv:1103.0455)
McCammon D., Burrows D. N., Sanders W. T., Kraushaar W. L., 1983, ApJ, 269, 107
Mou G., Yuan F., Bu D., Sun M., Su M., 2014, ApJ, 790, 109
Page L. et al., 2007, ApJS, 170, 335
Puspitarini L., Lallement R., Vergely J.-L., Snowden S. L., 2014, A&A, 566, A13
Racine R., 1968, AJ, 73, 233
Snowden S. L. et al., 1997, ApJ, 485, 125
Sofue Y., 1977, A&A, 60, 327

Sofue Y., 1984, PASJ, 36, 539
Sofue Y., 1994, ApJ, 431, L91
Sofue Y., 2000, ApJ, 540, 224
Sofue Y., Reich W., 1979, A&AS, 38, 251
Straižys V., Černis K., Bartašiūtė S., 2003, A&A, 405, 585
Strom S. E., Grasdalen G. L., Strom K. M., 1974, ApJ, 191, 111
Su M., Slatyer T. R., Finkbeiner D. P., 2010, ApJ, 724, 1044
Sun X. H., Gaensler B. M., Carretti E., Purcell C. R., Staveley-Smith L., Bernardi G., Haverkorn M., 2014, MNRAS, 437, 2936
Taylor A. R., Stil J. M., Sunstrum C., 2009, ApJ, 702, 1230

Weaver H. F., 1949, ApJ, 110, 190
Willingale R., Hands A. D. P., Warwick R. S., Snowden S. L., Burrows D. N., 2003, MNRAS, 343, 995
Wolleben M., 2007, ApJ, 664, 349
Zhang C. Y., Laureijs R. J., Wesselius P. R., Clark F. O., 1988, A&A, 199, 170

This paper has been typeset from a TEX/LATEX file prepared by the author.